Numerical Heat Transfer, Part B, 42: 141–166, 2002

1040-7790/02 $12.00 + .00
DOI: 10.1080/10407790190053879

# DISCUSSION ON MOMENTUM INTERPOLATION METHOD FOR COLLOCATED GRIDS OF INCOMPRESSIBLE FLOW

***Bo Yu, Wen-Quan Tao, and Jin-Jia Wei***
*Xi'an Jiaotong University, Xi'an, People's Republic of China*

***Yasuo Kawaguchi***
*Turbomachinery Research Group, Institute for Energy Utilization, National Institute of Advanced Industrial Science and Technology, Tsukuba, Ibaraki, Japan*

***Toshio Tagawa and Hiroyuki Ozoe***
*Institute of Advanced Material Study, Kyushu University, Kasuga, Fukuoka, Japan*

***Discussions are given of the different momentum interpolation methods to evaluate the interface velocity in the collocated grid system. It is pointed out that the interface velocity is used in three cases in the overall numerical procedure of the solution of Navier-Stokes equations by utilizing a collocated grid: in the continuity equation; in the interface flow rate computation for the determination of the coefficients in discretization equation; and in the mass residual in the coefficient $A_P$. Analysis shows that it is better to adopt the momentum interpolation method in the three cases. Two new momentum interpolation methods, called MMIM1 and MMIM2, are proposed. Analysis shows that the two new methods can achieve numerical solutions that are independent of both the underrelaxation factor and the time step size. Taking lid-driven cavity flow as an example, numerical computations are conducted for several Reynolds numbers and different mesh sizes using the SIMPLE algorithm, and the results are compared with benchmark solutions. Numerical tests demonstrate that both MMIM1 and MMIM2 can give unique solutions for different underrelaxation factors and time step sizes, solutions from MMIM1 are slightly better than that of the momentum interpolation of Majumdar, and solutions from MMIM2 have an appreciably better accuracy when the mesh is not fine.***

## INTRODUCTION

The SIMPLE-series algorithm of the control-volume discretization approach has been used extensively to solve incompressible fluid flow and heat transfer problems. Any computational domain can be divided into a finite number of contiguous nonoverlapping control volumes. Each control volume possesses its own grid. There

Received 10 August 2001; accepted 31 January 2002.
The second author greatly acknowledges the support from the National Project of Fundamental R&D of China (Grant 2000026303).
Address correspondence to Bo Yu, Mechanical Engineering Lab, Industrial Science & Technology, Ministry of Economy, Trade & Industrial, 1-2 Namiki, Tsukuba, Ibaraki 305-8564, Japan. E-mail: yubobox@hotmail.com

## NOMENCLATURE

| | |
|---|---|
| $A_P$, $A_E$, $A_W$, $A_N$, $A_S$ | coefficients in the finite-difference equation |
| $b$ | source term |
| $k$ | thermal conductivity |
| $L$ | characteristic length of cavity |
| $p$ | pressure |
| $P$ | dimensionless pressure |
| $s$ | source term |
| Re | Reynolds number |
| $t$ | time |
| $T$ | temperature |
| $u$, $v$ | velocity components in $x$ and $y$ coordinates |
| $U$, $V$ | dimensionless velocity components |
| $x$, $y$ | spatial coordinates |
| $X$, $Y$ | dimensionless coordinates |
| $\alpha$ | underrelaxation factor |
| $\Gamma$ | generalized diffusion coefficient |
| $\Delta x$, $\Delta y$ | cell dimensions |
| $\mu$ | viscosity |
| $\rho$ | density |
| $\phi$ | general variable |
| $\tau$ | dimensionless time |

**Superscripts**

| | |
|---|---|
| 0 | previous iteration |
| $l$ | last time step |

**Subscripts**

| | |
|---|---|
| e, w, n, s | cell faces |
| EE, E, W, WW, P, N, S | grid points |
| $T$, $u$, $v$ | refers to energy equation, and $u$, $v$ momentum equations, respectively |

are usually two kinds of grid arrangements: staggered grids and nonstaggered grids. For the nonstaggered grids, vector variables and scalar variables are stored at the same locations, while for the staggered grids, vector components and scalar variables are stored at different locations, being half a control-volume width apart in each coordinate. Staggered grids are popular because of their ability to prevent checkerboard pressure in the flow solution. The use of nonstaggered grids greatly reduces the required storage memory and shortens the computational time in three-dimensional calculations, especially for unstructured/curvilinear body-fitted grids. However, they are prone to produce a false pressure field—checkerboard pressure. For this reason, in the 1980s and before, nonstaggered grids were rarely used in the primitive variable method for incompressible flow. However, since 1983 the nonstaggered grid (or collocated grid) has been used more and more widely, after Rhie and Chow [1] proposed a momentum interpolation method to eliminate the checkerboard pressure and subsequent refinements by Peric [2] and Majumdar [3].

However, use of the original momentum interpolation (OMIM hereafter) proposed by Rhie and Chow may present additional problems. Majumdar [4] and Miller et al. [5] independently reported that solutions using the original Rhie and Chow scheme are underrelaxation factor-dependent. An iteration algorithm was proposed to remove the dependency [4]. Kobayashi et al. [6] presented a simple technique to remove the problem of underrelaxation factor dependence of the results by setting $\alpha_u = 1$ in the cell-face velocity expression. Choi [7] found that the original Rhie and Chow scheme is also time step size-dependent, and he proposed a modified scheme. He claimed that solutions from the modified scheme are independent of time step size. However, he did not show it mathematically as Majumdar did. Yu et al. [8] observed that the solutions from Choi's scheme are still time step size-dependent by a numerical example. They further showed that a checkerboard pressure field might be

obtained for small time step size and underrelaxation factor when using the OMIM of Rhie and Chow.

A more general pressure-correction algorithm for solution of incompressible Navier-Stokes equations was proposed in [9]. In that algorithm the cell-face velocities are evaluated by the linear interpolation of the two neighbor nodes. Rhie and Chow's scheme and various modified versions can be considered, in principle, a scheme to introduce a fourth-order dissipation into the pressure field to damp out the oscillation [10–12].

Performance comparisons between the staggered grid and nonstaggered arrangements have been reported in [5, 13–15]. These results show that SIMPLE-like algorithms on staggered grid and nonstaggered grid arrangements with the momentum interpolation method provide similarly accurate results and similar convergence rate. A new momentum interpolation was proposed in [16]. It was reported that the new scheme gives more accurate results than the OMIM.

To remove the pressure oscillation, another approach called SIMPLEN was proposed by Thiart [17, 18] and extended by Wang et al. [19]. This method is more complicated to implement and difficult to extend to a higher-order convective scheme. Therefore, it has not been used so much as Rhie and Chow's scheme.

In this article, comprehensive discussion will be made of the implementation of OMIM and new momentum interpolation methods will be introduced. In what follows, the transport equations to be solved for the lid-driven cavity flow are presented first. The original momentum interpolation method is briefly reviewed next. Detailed discussion is made of the three connections where interface velocities are needed. That the solution using Choi's scheme [7] is still time step size-dependent is analyzed. Two new momentum interpolation methods—MMIM1 and MMIM2—are proposed. Then numerical experiment results are presented to verify the above discussion. Finally, conclusions are drawn.

## MATHEMATICAL FORMULATION

Consider a two-dimensional incompressible laminar heat and fluid flow problem in a Cartesian coordinate with nonconstant properties. We have continuity equation

$$\frac{\partial(\rho u)}{\partial x} + \frac{\partial(\rho v)}{\partial y} = 0 \tag{1}$$

*u*-momentum equation

$$\frac{\partial(\rho u)}{\partial t} + \frac{\partial(\rho uu)}{\partial x} + \frac{\partial(\rho vu)}{\partial y} = -\frac{\partial p}{\partial x} + \frac{\partial}{\partial x}\left(\mu \frac{\partial u}{\partial x}\right) + \frac{\partial}{\partial y}\left(\mu \frac{\partial u}{\partial y}\right) + s_u \tag{2}$$

*v*-momentum equation

$$\frac{\partial(\rho v)}{\partial t} + \frac{\partial(\rho uv)}{\partial x} + \frac{\partial(\rho vv)}{\partial y} = -\frac{\partial p}{\partial y} + \frac{\partial}{\partial x}\left(\mu \frac{\partial v}{\partial x}\right) + \frac{\partial}{\partial y}\left(\mu \frac{\partial v}{\partial y}\right) + s_v \tag{3}$$

energy equation

$$\frac{\partial(\rho T)}{\partial t}+\frac{\partial(\rho u T)}{\partial x}+\frac{\partial(\rho v T)}{\partial y}=\frac{\partial}{\partial x}\left(k\frac{\partial T}{\partial x}\right)+\frac{\partial}{\partial y}\left(k\frac{\partial T}{\partial y}\right)+s_T \tag{4}$$

Equations (2)–(4) can be expressed in a general form:

$$\frac{\partial(\rho\phi)}{\partial t}+\frac{\partial(\rho u\phi)}{\partial x}+\frac{\partial(\rho v\phi)}{\partial y}=\frac{\partial}{\partial x}\left(\Gamma\frac{\partial\phi}{\partial x}\right)+\frac{\partial}{\partial y}\left(\Gamma\frac{\partial\phi}{\partial y}\right)+s_\phi \tag{5}$$

where $u$ and $v$ are the velocity components, $\phi$ is any dependent variable ($u$, $v$, and $T$), and $t$, $\rho$, $\Gamma$, and $s_\phi$ are time, density, diffusion coefficient, and source term, respectively. Note that for the continuity equation, $\phi = 1$, $\Gamma = 0$, and $s_\phi = 0$.

The finite-volume method is used to discretize the governing equation. A nonstaggered grid system in which all variables are stored at the center of the control volume is used (Figure 1).

Integrating Eq. (5) over the control volume with bounded cell faces e, w, n, and s surrounding center P, we have

$$\begin{aligned}\frac{\rho\,\Delta x\,\Delta y}{\Delta t}\left(\phi_{\mathrm{P}}-\phi_{\mathrm{P}}^{l}\right)+\left[(\rho u\phi)_{\mathrm{e}}-(\rho u\phi)_{\mathrm{w}}\right]\Delta y+\left[(\rho v\phi)_{\mathrm{n}}-(\rho v\phi)_{\mathrm{s}}\right]\Delta x\\ =\left[\frac{\Gamma_{\mathrm{e}}}{\delta x_{\mathrm{e}}}(\phi_{\mathrm{E}}-\phi_{\mathrm{P}})-\frac{\Gamma_{\mathrm{w}}}{\delta x_{\mathrm{w}}}(\phi_{\mathrm{P}}-\phi_{\mathrm{W}})\right]\Delta y+\left[\frac{\Gamma_{\mathrm{n}}}{\delta y_{\mathrm{n}}}(\phi_{\mathrm{N}}-\phi_{\mathrm{P}})-\frac{\Gamma_{\mathrm{s}}}{\delta y_{\mathrm{s}}}(\phi_{\mathrm{P}}-\phi_{\mathrm{S}})\right]\Delta x\\ +(s_c+S_p\phi_p)\,\Delta x\,\Delta y\end{aligned} \tag{6}$$

where the superscript $l$ refers to the previous time level, and $\Delta x$, $\Delta y$, $\delta x_{\mathrm{e}}$, $\delta x_{\mathrm{w}}$, $\delta y_{\mathrm{n}}$, and $\delta y_{\mathrm{s}}$ are geometric lengths as shown in Figure 1. The diffusive term is discretized by the central difference scheme and the source term is treated by linearization [20]. Many different schemes have been proposed to discretize the convective term, such as the first-order upwind difference scheme, the second-order upwind difference

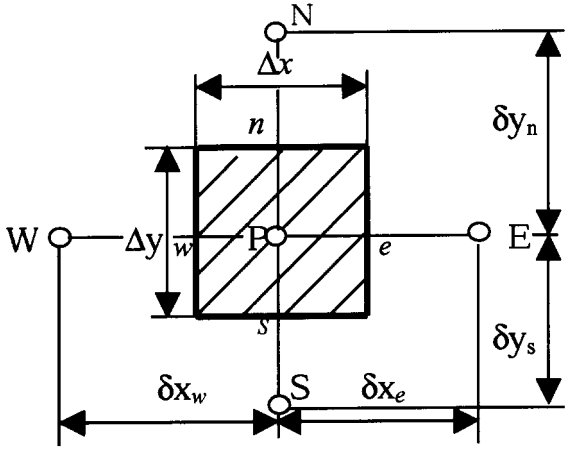


**Figure 1.** Nonstaggered grid arrangement.

scheme, the central difference scheme, and the QUICK scheme [21]. The QUICK scheme has been found to offer solutions with high accuracy and have good stability in the field of computational heat transfer. Thus in the present study this scheme is employed to discretize the convective term. According to Hayase et al. [22], the formula for the QUICK scheme for a cell face $e$ in Figure 2 can be expressed as

$$\phi_e = \begin{cases} \phi_P + \left(C_W^+ \phi_W + C_P^+ \phi_P + C_E^+ \phi_E\right) & u_e \geq 0 \\ \phi_E + \left(C_{EE}^- \phi_{EE} + C_E^- \phi_E + C_P^- \phi_P\right) & u_e < 0 \end{cases} \tag{7}$$

where

$$C_W^+ = -\frac{\Delta x_P \, \Delta x_E}{(\Delta x_W + \Delta x_P)(\Delta x_W + 2\Delta x_P + \Delta x_E)} \tag{8}$$

$$C_P^+ = \frac{(-\Delta x_W - \Delta x_P + \Delta x_E)\,\Delta x_P}{(\Delta x_W + \Delta x_P)(\Delta x_P + \Delta x_E)} \tag{9}$$

$$C_P^- = \frac{(2\Delta x_E + \Delta x_{EE})\,\Delta x_E}{(\Delta x_P + 2\Delta x_E + \Delta x_{EE})(\Delta x_P + \Delta x_E)} \tag{10}$$

$$C_E^+ = \frac{(\Delta x_W + 2\Delta x_P)\,\Delta x_P}{(\Delta x_W + 2\Delta x_P + \Delta x_E)(\Delta x_P + \Delta x_E)} \tag{11}$$

$$C_E^- = \frac{(\Delta x_P - \Delta x_E - \Delta x_{EE})\,\Delta x_E}{(\Delta x_P + \Delta x_E)(\Delta x_E + \Delta x_{EE})} \tag{12}$$

$$C_{EE}^- = -\frac{\Delta x_P \, \Delta x_E}{(\Delta x_E + \Delta x_{EE})(\Delta x_P + 2\Delta x_E + \Delta x_{EE})} \tag{13}$$

The cell dimensions $\Delta x_W$, $\Delta x_P$, $\Delta x_E$, and $\Delta x_{EE}$ are shown in Figure 2. Similar formulas can be written for the other three cell faces, w, n, and s. It is noted that on the right-hand side of Eqs. (7), the first term is the first-order upwind difference

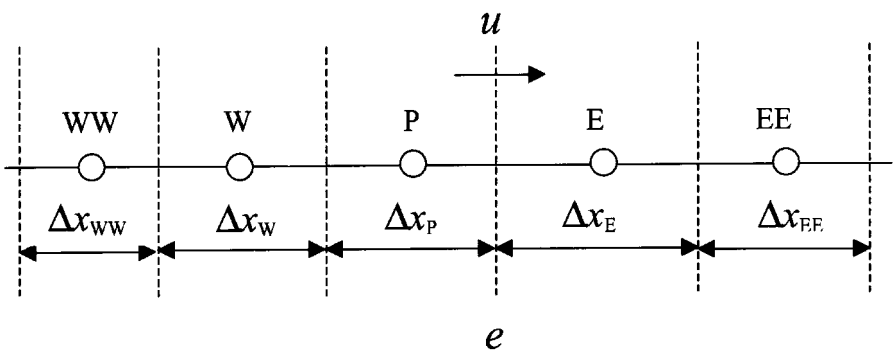


**Figure 2.** Grids in the $x$ direction.

scheme and the term in parentheses is the difference between the QUICK scheme and the first-order upwind scheme. The first term is used to form the discretized equation coefficients and the term in parentheses is incorporated in the source term. This approach was first reported by Khosla and Rubin [23] and is often called the deferred-correction technique in the literature. By using this technique, the resulting discretized equation is always diagonally dominant. The advantages of this technique have been addressed in [22].

The discretized continuity equation is

$$(\rho u)_e \Delta y - (\rho u)_w \Delta y + (\rho v)_n \Delta x - (\rho v)_s \Delta x = 0 \tag{14}$$

Substituting Eq. (7) for cell face $e$ and similar formulas for the other cell faces into Eq. (6) and rearranging, we obtain the final discretized equation for any general variable $\phi$ as follows:

$$A_P \phi_P = A_E \phi_E + A_W \phi_W + A_N \phi_N + A_S \phi_S + A_P^l \phi_P^l + b_P \tag{15}$$

where

$$\begin{aligned}
A_E &= \frac{\Gamma_e \Delta y}{\delta x_e} + \max\left[-(\rho u)_e \Delta y, 0\right] \qquad A_W = \frac{\Gamma_w \Delta y}{\delta x_w} + \max\left[(\rho u)_w \Delta y, 0\right] \\
A_N &= \frac{\Gamma_n}{\delta y_n} + \max\left[-(\rho v)_n \Delta x, 0\right] \qquad A_S = \frac{\Gamma_s}{\Delta y_s} + \max\left[(\rho v)_s \Delta x, 0\right] \\
A_P^l &= \frac{\rho \Delta x \Delta y}{\Delta t} \qquad A_P = A_E + A_W + A_N + A_S + A_P^l - s_P \Delta x \Delta y + A_b \\
A_b &= (\rho u)_e \Delta y - (\rho u)_w \Delta y + (\rho v)_n \Delta x - (\rho v)_s \Delta x \\
b_P &= s_c \Delta x \Delta y + b_1 \\
b_1 &= -\max\left[(\rho u)_e \Delta y, 0\right](\phi_e - \phi_P) + \max\left[-(\rho u)_e \Delta y, 0\right](\phi_e - \phi_E) \\
&\quad - \max\left[-(\rho u)_w \Delta y, 0\right](\phi_w - \phi_P) + \max\left[(\rho u)_w \Delta y, 0\right](\phi_w - \phi_W) \\
&\quad - \max\left[(\rho v)_n \Delta x, 0\right](\phi_n - \phi_P) + \max\left[-(\rho v)_n \Delta x, 0\right](\phi_n - \phi_N) \\
&\quad - \max\left[-(\rho v)_s \Delta x, 0\right](\phi_s - \phi_P) + \max\left[(\rho v)_s \Delta x, 0\right](\phi_s - \phi_S)
\end{aligned} \tag{16}$$

where the term $b_1$ results from the adoption of the deferred-correction procedure. It should be noted that for the velocity components, $u$ and $v$, the related pressure gradient term is temporarily buried in the source term $S_c$. From Eqs. (14) and (16) we can clearly see that the interface velocities ($u_e$, $u_w$, $v_n$, $v_s$) are used in three cases: in the continuity equation; in the interface flow rate computations for the determination of the coefficients in discretization equation; and in the mass residual $A_b$ in the coefficient $A_P$. $A_b$ is usually dropped, since divergence-free conditions are always required for the velocity field.

In order to slow down the changes of dependent variables in consecutive solutions, an underrelaxation factor is introduced into the discretized equations as follows [20]:

$$\begin{aligned}\phi_P &= \frac{\alpha_\phi}{A_P}\left(A_E\phi_E + A_W\phi_W + A_N\phi_N + A_S\phi_S + b_P + A_P^l\phi_P^l\right) + \left(1-\alpha_\phi\right)\phi_p^0 \\ &= \frac{\alpha_\phi}{A_P}\left(A_E\phi_E + A_W\phi_W + A_N\phi_N + A_S\phi_S + B_P\right)\end{aligned} \tag{17}$$

where the superscript 0 refers to the previous iteration and

$$B_P = b_P + A_P^l\phi_P^l + \frac{\left(1-\alpha_\phi\right)}{\alpha_\phi}A_P\phi_p^0 \tag{18}$$

## MOMENTUM INTERPOLATION AND DISCUSSION

### Momentum Interpolation for Steady-State Problem

By taking out the pressure gradient term from the source term, Eq. (17) for velocity component $u$ at nodes $P$ and $E$ can be rewritten as

$$u_P = \frac{\alpha_u\left(\sum_i A_i u_i + B_P\right)_P}{(A_P)_P} - \frac{\alpha_u\,\Delta y(p_e - p_w)_P}{(A_P)_P} \tag{19}$$

$$u_E = \frac{\alpha_u\left(\sum_i A_i u_i + B_P\right)_E}{(A_P)_E} - \frac{\alpha_u\,\Delta y(p_e - p_w)_E}{(A_P)_E} \tag{20}$$

Mimicking the formulation of $u_E$ and $u_P$, we can obtain following expression for the interface velocity at the cell face $e$:

$$u_e = \frac{\alpha_u\left(\sum_i A_i u_i + B_P\right)_e}{(A_P)_e} - \frac{\alpha_u\,\Delta y(p_E - p_P)}{(A_P)_e} \tag{21}$$

where the terms on the right-hand side with subscript e should be interpolated in an appropriate manner. The interface velocity at cell faces w, n, and s can be obtained similarly, and in what follows discussion is given only for $u_e$, for the sake of simplicity.

In Rhie and Chow's momentum interpolation, the first term and $1/(A_P)_e$ in the second term of Eq. (21) are linearly interpolated from their counterparts in Eqs. (19) and (20):

$$\left(\frac{\sum_i A_i u_i + B_P}{A_P}\right)_e = f_e^+\left(\frac{\sum_i A_i u_i + B_P}{A_P}\right)_E + \left(1-f_e^+\right)\left(\frac{\sum_i A_i u_i + B_P}{A_P}\right)_P \tag{22}$$

$$\frac{1}{(A_P)_e} = f_e^+\frac{1}{(A_P)_E} + \left(1-f_e^+\right)\frac{1}{(A_P)_P} \tag{23}$$

where $f_e^+$ is a linear interpolation factor defined as

$$f_e^+ = \frac{\Delta x_P}{2\delta x_e} \tag{24}$$

Equations (22) and (23) constitute the OMIM. Majumdar [4] reported that solutions of steady-state problems from the Rhie and Chow OMIM are dependent

on the underrelaxation factor. To eliminate this underrelaxation factor dependence, an iteration algorithm was proposed by him to calculate the cell-face velocity for the steady-state problem as follows:

$$u_e = \frac{\alpha_u \left(\sum_i A_i u_i + B_P\right)_e}{(A_P)_e} - \frac{\alpha_u \Delta y (p_E - p_P)}{(A_P)_e} + (1 - \alpha_u)[u_e^0 - f_e^+ u_E^0 - (1 - f_e^+) u_P^0] \quad (25)$$

Note that $B_P = b_P + [(1 - \alpha_u)/\alpha_u] A_P u_p^0$ [Eq. (18)] for the steady problem. This iterative implementation algorithm can achieve a unique solution that is independent of underrelaxation factors, which will be demonstrated later. In order to have a better understanding of Eq. (25), substituting $[(\sum_i A_i u_i + B_P)/A_P]_e$ from Eq. (22) and $[(\sum_i A_i u_i + B_P)/A_P]_P$, $[(\sum_i A_i u_i + B_P)/A_P]_E$ from Eqs. (19) and (20) into Eq. (25), and omitting the term $A_P^l u_P^l$, we obtain

$$u_e = [f_e^+ u_E + (1 - f_e^+) u_P] + \left\{ \begin{array}{l} -\frac{\alpha_u \Delta y (p_E - p_P)}{(A_P)_e} + f_e^+ \frac{\alpha_u \Delta y (p_e - p_w)_E}{(A_P)_E} + (1 - f_e^+) \\ \times \frac{\alpha_u \Delta y (p_e - p_w)_P}{(A_P)_P} + (1 - \alpha_u)[u_e^0 - f_e^+ u_E^0 - (1 - f_e^+) u_P^0] \end{array} \right\} \quad (26)$$

Equations (25) and (26) are essentially equivalent. However, Eq. (26) separates the interfacial velocity into two parts: a linear interpolation part and the additional one. In the following, the meanings of the two parts and the roles of the interface velocity will be discussed in detail.

### Discussion 1: Roles of the Interface Velocity

The term in the first set of brackets of Eq. (26) is the arithmetic-averaged values (linear interpolation method) of two neighbor nodal velocities. The term in braces can be regarded as a correction term, which has the function of smoothing the pressure field, and it is this term that may remove the unrealistic pressure field. In this regard, the above interface velocity plays a role of coupling between velocity and pressure (coupling role). In addition, when the coefficient of the discretization equation is determined by whatever scheme, the interface velocity is also needed to determine the flow rate. Different flow rates at the cell faces will lead to different coefficients, hence different solutions. This is the scheme role of the interface velocity. And what was found by Majumdar in [4] is that in the OMIM the interface flow rate depends on the underrelaxation factor. Another important role of the interface velocity is that it appears in the $A_b$ of Eq. (16), which should be always near zero to enhance the robustness of the solution procedure (mass balance role). Now comes a very important but tough problem for the collocated grids: what is the exact expression for the interface velocity? Unfortunately, for the collocated grid, there is no strict way to determine the interface velocity [24]. We have to make some compromise among the importance of three roles. First, the checkerboard pressure field should be avoided, and for this purpose, OMIM is our choice. Second, the solutions should be independent of the underrelaxation factor and the time step size, thus the OMIM should be improved to meet this requirement, and this is one of the major purpose of the present study. Third, for the discretization coefficient, another interpolation method (say, linear interpolation) may be adopted for the interface

velocity, as has been done by Date [9]. However, this will violate mass balance in Eq. (16), since momentum interpolation is used for the continuity equation. As we mentioned before, the term $A_b$ in Eq. (16) is usually dropped in the literatures. But it cannot be dropped if the arithmetic mean velocities are employed to evaluate the convective coefficients. This is because the cell-face velocities calculated by Eqs. (25)/(26) are enforced to satisfy the continuity equation, which makes the arithmetic-mean cell-face velocities [the first bracketed term in Eq. (26)] not satisfy the continuity equation. Thus $A_b$ should be retained. If we retain $A_b$, then the coefficient $A_P$ may be less than the summation of its neighbor coefficients, an important characteristic to ensure the convergence of the iterative solution procedure of the algebraic equations. In addition, the existence of the $A_b$ term actually means that mass conservation is not satisfied in the discretized equations for both scalar and velocity variables, which may reduce the solution accuracy. On the other hand, if the term $A_b$ is dropped, the solution may also be affected, since for this case the discretization equation is not exactly the one we expected by using the specified schemes. From the above analysis, it can be seen that for the interface velocity it is better to use the same interpolation method in its three roles for the whole numerical procedure.

Of course, the validity of the momentum interpolation depends heavily on the basic assumptions adopted in the momentum interpolation, i.e., Eqs. (22) and (23). It has been found that in the region with large pressure gradient the cell-face velocity by momentum interpolation sometimes does not remain bounded between the two neighbor nodal velocities [5]. We also observed such a phenomenon in the calculations of high-Reynolds/Rayleigh-number problems. This may be viewed as the penalty we pay for some special cases when we use the momentum interpolation method. In test 1 of the subsequent test section we compare the performance of three practices (A, B, and C) in the computation of lid-driven cavity flow. In practice A the interface velocity determined by the MIM of Majumdar [Eq. (25)] is used for both the continuity equation and the coefficient of the discretization equation. In practice B the MIM of Majumdar is used in the discretized continuity equation but linear interpolation is used in the flow rate for the coefficient of discretized momentum equation. In practices A and B the term $A_b$ of Eq. (16) is dropped. Practice C is the same as practice B except that in practice C the term $A_b$ remains in the computational process. From our numerical experiments, speaking in general, the momentum interpolation (actually, its improved version) is recommended for adoption for the interface velocity in the three roles.

### Discussion 2: Two New Momentum Interpolations for Unsteady Problems

As mentioned above, Choi [7] reported that the solution using the original Rhie and Chow scheme is time step size-dependent. He proposed a modified Rhie and Chow scheme for an unsteady problem as follows, which is quite similar to Majumdar's scheme for a steady problem:

$$u_e = \alpha_u \left( \frac{\sum_i A_i u_i + b_P}{A_P} \right)_e - \frac{\alpha_u \Delta y (p_E - p_P)}{(A_P)_e} + (1 - \alpha_u) u_e^0 + \frac{\alpha_u A_e^l}{(A_P)_e} u_e^l \qquad (27)$$

with

$$A_e^l = \frac{\rho\, \delta x_e\, \Delta y}{\Delta t} \tag{28}$$

It is to be noted that the body-force term is neglected in this article for simplicity of presentation. By a similar substitution process as the one for the Majumdar's interpolation, Eq. (25), Eq. (27) can be written equivalently as

$$u_e = [f_e^+ u_E + (1 - f_e^+) u_P] + \left\{ \begin{array}{l} -\frac{\alpha_u \Delta y (p_E - p_P)}{(A_P)_e} + f_e^+ \frac{\alpha_u \Delta y (p_e - p_w)_E}{(A_P)_E} + (1 - f_e^+) \\ \times \frac{\alpha_u \Delta y (p_e - p_w)_P}{(A_P)_P} + (1 - \alpha_u)[u_e^0 - f_e^+ u_E^0 - (1 - f_e^+) u_P^0] \\ + \left[ \frac{\alpha_u A_e^l}{(A_P)_e} u_e^l - f_e^+ \frac{\alpha_u (A_P^l)_E}{(A_P)_E} u_E^l - (1 - f_e^+) \frac{\alpha_u (A_P^l)_P}{(A_P)_P} u_P^l \right] \end{array} \right\} \tag{29}$$

Choi claimed that using his modified scheme the solution is independent of time step size, and he showed it by a numerical example. We observed that his monitored velocity value, Eq. (27), is still dependent on time step size, though the difference is quite small. We believe that the observed slight difference is probably not due to computational error, but arises from the scheme itself. We now show this time step size dependency analytically as follows. For simplicity, we start our analysis from Eq. (27).

When a steady converged solution is reached, we have $u_e = u_e^0 = u_e^l$, $u_E = u_E^0 = u_E^l$, and $u_P = u_P^0 = u_P^l$. Then Eq. (27) can be written as

$$u_e = \alpha_u \left( \frac{\sum_i A_i u_i + b_P}{A_P} \right)_e - \frac{\alpha_u \Delta y (p_E - p_P)}{(A_P)_e} + (1 - \alpha_u) u_e + \frac{\alpha_u A_e^l}{(A_P)_e} u_e \tag{30}$$

Then

$$u_e = \left( \frac{\sum_i A_i u_i + b_P}{A_P} \right)_e - \frac{\Delta y (p_E - p_P)}{(A_P)_e} + \frac{A_e^l}{(A_P)_e} u_e \tag{31}$$

that is,

$$u_e = \frac{(A_P)_e [(\sum_i A_i u_i + b_P)/A_P]_e - \Delta y (p_E - p_P)}{(A_P)_e - A_e^l} \tag{32}$$

Similar to Eq. (22),

$$\begin{aligned} \left( \frac{\sum_i A_i u_i + b_P}{A_P} \right)_e &= f_e^+ \left( \frac{\sum_i A_i u_i + b_P}{A_P} \right)_E + (1 - f_e^+) \left( \frac{\sum_i A_i u_i + b_P}{A_P} \right)_P \\ &= \frac{f_e^+ (\sum_i A_i u_i + b_P)_E (A_P)_P + (1 - f_e^+)(\sum_i A_i u_i + b_P)_P (A_P)_E}{(A_P)_P (A_P)_E} \end{aligned} \tag{33}$$

And from Eq. (23), we have

$$(A_P)_e = \frac{(A_P)_P (A_P)_E}{f_e^+ (A_P)_P + (1 - f_e^+)(A_P)_E} \tag{34}$$

Substituting Eqs. (33) and (34) into Eq. (32), we obtain

$$u_e = \frac{\left[f_e^+\left(\sum_i A_i u_i + b_P\right)_E (A_P)_P + (1-f_e^+)\left(\sum_i A_i u_i + b_P\right)_P (A_P)_E\right] - \Delta y[f_e^+ (A_P)_P + (1-f_e^+)(A_P)_E](p_E - p_P)}{(A_P)_P (A_P)_E - (f_e^+ (A_P)_P + (1-f_e^+)(A_P)_E) A_e^l} \tag{35}$$

On the right-hand side of the expression, the parameters and variables are apparently independent of underrelaxation factor $\alpha_u$. That means $u_e$ is independent of $\alpha_u$. Thus the converged solution is independent of velocity underrelaxation factor. This conclusion is consistent with that in [4]. However, we can see that $u_e$ is dependent on time step size $\Delta t$ because $\Delta t$ is included in the coefficients $(A_P)_P$, $(A_P)_E$, and $A_e^l$. Therefore the converged solution is dependent on $\Delta t$. Furthermore, the function between $u_e$ and $\Delta t$ is nonlinear and complicated, hence no explicit variation trend can be revealed between $u_e$ and $\Delta t$ from Eq. (35). A numerical case in test 2 of the subsequent test section is presented to verify our analysis.

In the literature, other interpolation schemes for the interface velocity may be found. But to the knowledge of the present authors, no existing schemes can eliminate the effects of both the underrelaxation factor and time step size. For example, Issa and Oliveira [25] proposed a modified momentum interpolation in a dispersed two-phase flow simulation as follows:

$$u_e = \frac{\alpha_u f_e^+ \left(\sum_i A_i u_i + B_P\right)_E + \alpha_u (1-f_e^+)\left(\sum_i A_i u_i + B_P\right)_P - \alpha_u \Delta y (P_E - P_P)}{f_e^+ (A_P)_E + (1-f_e^+)(A_P)_P} \tag{36}$$

This scheme has also been used successfully in the simulation of viscoelastic flows [26]. However, solutions by using this scheme are also underrelaxation factor- and time step size-dependent.

The feature that the converged solution is dependent on time step size is undesirable. It motivates us to propose a modified scheme to eliminate such a drawback.

In the following we propose a scheme to remove those effects, based on Eq. (27) and Eq. (36). First, we interpolate the first term on the right-hand side of Eq. (27) as follows:

$$\left(\frac{\sum_i A_i u_i + b_P}{A_P}\right)_e = \frac{f_e^+ (\sum_i A_i u_i + b_1)_E + (1-f_e^+)\left(\sum_i A_i u_i + b_1\right)_P + [f_e^+ (S_c)_E + (1-f_e^+)(S_c)_P]\delta x_e \Delta y}{f_e^+ \left(\sum_i A_i\right)_E + (1-f_e^+)\left(\sum_i A_i\right)_P - [f_e^+ (S_P)_E + (1-f_e^+)(S_P)_P]\delta x_e \Delta y + A_e^l} \tag{37}$$

where $b_1$ is defined in Eq. (16).

Second, the denominator of the second and third terms in Eq. (27) is interpolated as follows:

$$(A_P)_e = f_e^+ \left(\sum_i A_i\right)_E + (1-f_e^+)\left(\sum_i A_i\right)_P - \left[f_e^+ (S_P)_E + (1-f_e^+)(S_P)_P\right]\delta x_e \Delta y + A_e^l \tag{38}$$

Note that the discussions in the former section, "Discussion 1," have shown that practice A is better to use. So in this section, practice A is used. Then $(A_b)_e$ in the

coefficient $(A_P)_e$ has been dropped as shown in the above equation. Equation (27) combined with Eq. (37) and Eq. (38) is our new scheme.

Then, substituting Eq. (37) into Eq. (27), we obtain

$$u_e = \frac{1}{(A_P)_e}\left\{\begin{array}{l}[f_e^+(A_P)_E u_E + (1-f_e^+)(A_P)_P u_P] \\ + \alpha_u[(f_e^+(S_c)_E + (1-f_e^+)(S_c)_P)\,\delta x_e\,\Delta y \\ - f_e^+(S_c)_E\,\Delta x_E\,\Delta y - (1-f_e^+)(S_c)_P\,\Delta x_P\,\Delta y] \\ + \alpha_u[-\Delta y(p_E - p_P) + f_e^+\,\Delta y(p_e - p_w)_E \\ +(1-f_e^+)\Delta y(p_e - p_w)_P] \\ + (1-\alpha_u)[u_e^0 - f_e^+ u_E^0 - (1-f_e^+)u_P^0] \\ + \alpha_u[A_e^l u_e^l - f_e^+(A_P^l)_E u_E^l - (1-f_e^+)(A_P^l)_P u_P^l]\end{array}\right\} \tag{39}$$

where $(A_P)_e$ is determined by Eq. (38).

Now let us show that the above scheme for the interface velocity can make the solution independent of time step size. When a steady converged solution is reached, Eq. (27) changes into Eq. (32), as shown before. As for showing the dependency of time step size of Choi's interpolation scheme, we also use Eq. (32) to demonstrate the independency of time step size of the above interpolation method. By substituting Eqs. (37) and (38) into Eq. (32), we obtain

$$u_e = \frac{\begin{array}{c}f_e^+\left(\sum_i A_i u_i + b_1\right)_E + (1-f_e^+)\left(\sum_i A_i u_i + b_1\right)_P \\ + [f_e^+(S_c)_E + (1-f_e^+)(S_c)_P]\delta x_e \Delta y - \Delta y(P_E - P_P)\end{array}}{f_e^+\left(\sum_i A_i\right)_E + \left(1-f_e^+\right)\left(\sum_i A_i\right)_P - \left[f_e^+(S_P)_E + \left(1-f_e^+\right)(S_P)_P\right]\delta x_e \Delta y} \tag{40}$$

Since on the right-hand side of Eq. (40) all parameters and variables are independent of underrelaxation factor $\alpha_u$ and time step size $\Delta t$, the converged solution is independent of both $\alpha_u$ and $\Delta t$. For convenience, this scheme is called MMIM1 hereafter.

In [16], a quadratic interpolation formula (full QUICK scheme) was employed to determine all the interface terms in Eq. (21). The scheme was called QMIM. For a one-dimensional situation, the cell-face velocity is obtained from three consecutive values: two neighbor nodes plus the adjacent node on the upstream side. It was reported that QMIM can predict more accurate results than the OMIM scheme and achieve a faster convergence rate. In the following we propose a new scheme in which the interface quantity is obtained from four neighbor nodes, two upstream and two downstream, hence it can be regarded as a fourth-order scheme. The interfacial terms in Eq. (21) are interpolated as follows:

$$\left(\frac{\sum_i A_i u_i + b_P}{A_P}\right)_e = \frac{\left(\sum_i A_i u_i + b_1\right)_e + (S_c)_e\,\delta x_e\,\Delta y}{\left(\sum_i A_i\right)_e - (S_p)_e\,\delta x_e\,\Delta y + A_e^l} \tag{41}$$

$$\left(\sum_i A_i u_i + b_1\right)_e = C_{EE}\left(\sum_i A_i u_i + b_1\right)_{EE} + C_E\left(\sum_i A_i u_i + b_1\right)_E + C_P\left(\sum_i A_i u_i + b_1\right)_P + C_W\left(\sum_i A_i u_i + b_1\right)_W \tag{42}$$

$$(S_c)_e = C_{EE}(S_c)_{EE} + C_E(S_c)_E + C_P(S_c)_P + C_W(S_c)_W \tag{43}$$

$$(A_P)_e = \left(\sum_i A_i\right)_e - (S_p)_e\,\delta x_e\,\Delta y + A_e^l \tag{44}$$

$$\left(\sum_i A_i\right)_e = C_{EE}\left(\sum_i A_i\right)_{EE} + C_E\left(\sum_i A_i\right)_E + C_P\left(\sum_i A_i\right)_P + C_W\left(\sum_i A_i\right)_W \tag{45}$$

$$(S_P)_e = C_{EE}(S_P)_{EE} + C_E(S_P)_E + C_P(S_P)_P + C_W(S_P)_W \tag{46}$$

where

$$C_{EE} = -\frac{(\Delta x_W + 2\Delta x_P)\,\Delta x_P\,\Delta x_E}{(\Delta x_W + 2\Delta x_P + 2\Delta x_E + \Delta x_{EE})(\Delta x_P + 2\Delta x_E + \Delta x_{EE})(\Delta x_E + \Delta x_{EE})} \tag{47}$$

$$C_E = \frac{(\Delta x_W + 2\Delta x_P)\Delta x_P(2\Delta x_E + \Delta x_{EE})}{(\Delta x_W + 2\Delta x_P + \Delta x_E)(\Delta x_P + \Delta x_E)(\Delta x_E + \Delta x_{EE})} \tag{48}$$

$$C_P = \frac{(\Delta x_W + 2\Delta x_P)\Delta x_E(2\Delta x_E + \Delta x_{EE})}{(\Delta x_W + \Delta x_P)(\Delta x_P + \Delta x_E)(\Delta x_P + 2\Delta x_E + \Delta x_{EE})} \tag{49}$$

$$C_W = -\frac{\Delta x_P \Delta x_E(2\Delta x_E + \Delta x_{EE})}{(\Delta x_W + \Delta x_P)(\Delta x_W + 2\Delta x_P + \Delta x_E)(\Delta x_W + 2\Delta x_P + 2\Delta x_E + \Delta x_{EE})} \tag{50}$$

This scheme is called MMIM2 hereafter. For the cell face next to the boundary, Eqs. (37) and (38) are used. Similar analysis shows that the solution using MMM2 is independent of both the underrelaxation factor and time step size. A numerical case in test 2 of the subsequent test section is presented to show that solutions from MMIM1 and MMIM2 are independent of both the underrelaxation factor and time step size.

## TEST

The well-known lid-driven cavity flow is used as a test problem as depicted in Figure 3. The Reynolds number is defined by $\mathrm{Re} = \rho U_{lid} L/\mu$, where $U_{lid}$ is the velocity of the top moving wall and $L$ is the length of the square cavity. The dimensionless governing equations for the test problem are

$$\frac{\partial U}{\partial X} + \frac{\partial V}{\partial Y} = 0 \tag{51}$$

$$\frac{\partial U}{\partial \tau} + \frac{\partial UU}{\partial X} + \frac{\partial VU}{\partial Y} = -\frac{\partial P}{\partial X} + \frac{1}{\mathrm{Re}}\left(\frac{\partial^2 U}{\partial X^2} + \frac{\partial^2 U}{\partial Y^2}\right) \tag{52}$$

$$\frac{\partial V}{\partial \tau} + \frac{\partial UV}{\partial X} + \frac{\partial VV}{\partial Y} = -\frac{\partial P}{\partial Y} + \frac{1}{\mathrm{Re}}\left(\frac{\partial^2 V}{\partial X^2} + \frac{\partial^2 V}{\partial Y^2}\right) \tag{53}$$

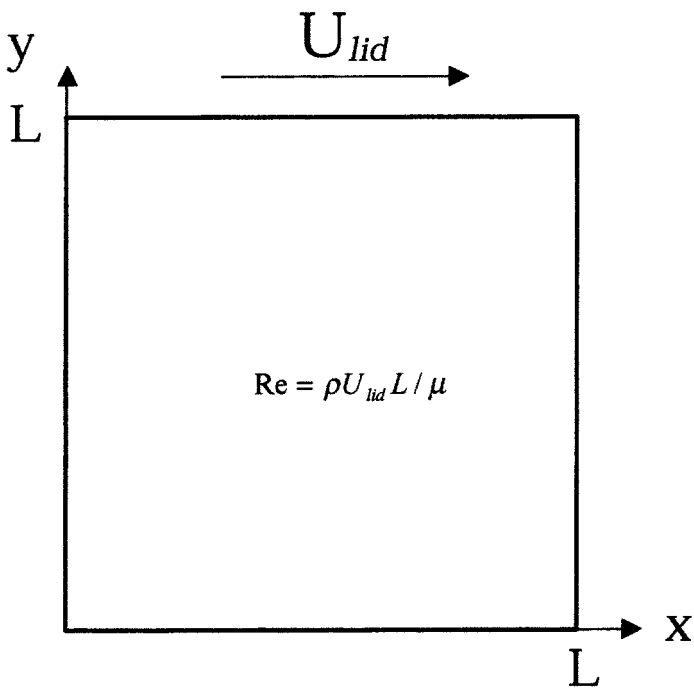


**Figure 3.** Lid-driven cavity flow.

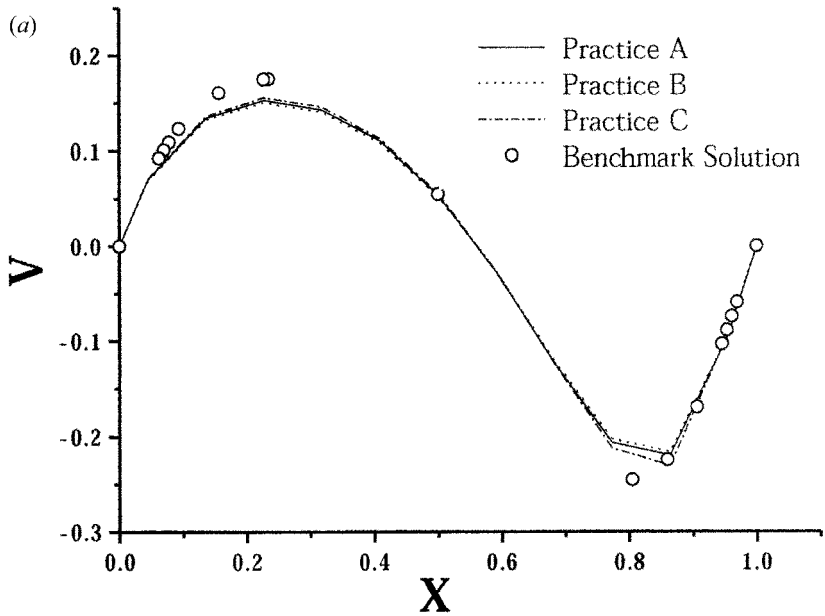


**Figure 4*a*.** Velocity profiles along the horizontal cavity centerline for practices A, B, and C using a 13 × 13 uniform mesh: (*a*) Re = 100.

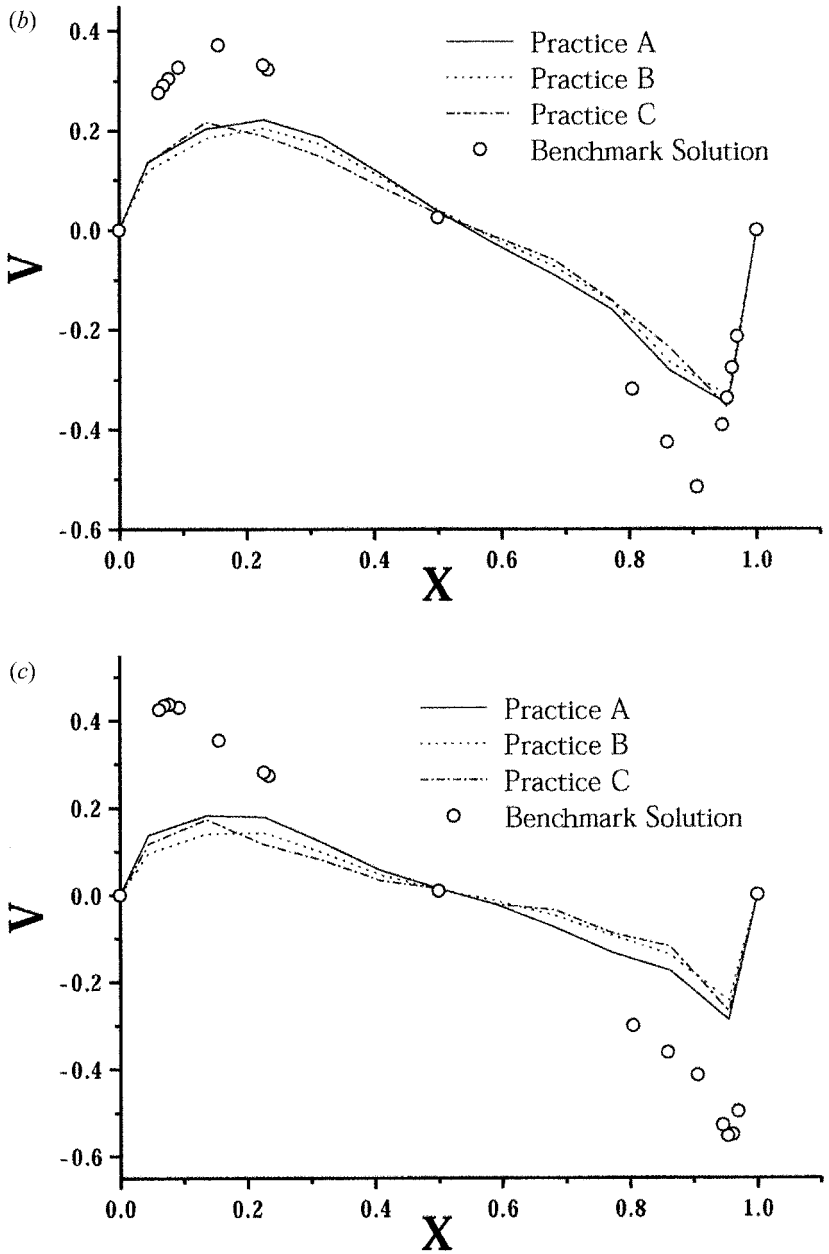


**Figure 4*b–c*.** Velocity profiles along the horizontal cavity centerline for practices A, B, and C using a $13 \times 13$ uniform mesh: (*b*) Re = 1,000; (*c*) Re = 5,000.

In the above equations, the following dimensionless variables are introduced:

$$\tau = \frac{tU_{\text{lid}}}{L} \qquad X = \frac{x}{L} \qquad Y = \frac{y}{L} \qquad \text{Re} = \rho U_{\text{lid}} \frac{L}{\mu}$$
$$U = \frac{u}{U_{\text{lid}}} V = \frac{v}{U_{\text{lid}}} \qquad P = \frac{p}{\rho U_{\text{lid}}^2} \tag{54}$$

The discretized algebraic equations are solved by a line-by-line alternating direction implicit (ADI) method. When the residuals for the continuity equation, $u$-momentum equation, and $v$-momentum equation are less than $1.0 \times 10^{-8}$, convergence solutions are assumed to be achieved and calculations are terminated. The mass residual is

$$\text{Re}\, s_m = \left|(\rho u)_{\text{e}} \Delta y - (\rho u)_{\text{w}} \Delta y + (\rho v)_{\text{n}} \Delta x - (\rho v)_{\text{s}} \Delta x\right|_{\max} \tag{55}$$

It should be noted that in Eq. (55), the interface velocity components are evaluated by momentum interpolation.

The residual for a general variable $\phi$ is defined as

$$\text{Re}\, s_\phi = \frac{\sqrt{\sum \left(A_{\text{P}}\phi_{\text{p}} - A_{\text{E}}\phi_{\text{E}} - A_{\text{W}}\phi_{\text{W}} - A_{\text{N}}\phi_{\text{N}} - A_{\text{S}}\phi_{\text{S}} - A_{\text{P}}^{l}\phi_{\text{P}}^{l} - b_{\text{P}}\right)^2}}{\sqrt{\sum \left(A_{\text{p}}\phi_{\text{p}}\right)^2}} \tag{56}$$

### Test 1

For practices A, B, and C, calculations are made for Re = 100, 1,000, and 5,000. A uniform grid of $13 \times 13$ meshes is used. Figure 4 shows the predicted vertical velocity profiles along the horizontal cavity centerline. The benchmark solutions of Ghia et al. [27] are also shown. The comparisons show that practice A is more accurate than practice B for the three Reynolds numbers. Practice C is most accurate for Re = 100. But for Re = 1,000 and 5,000, the performance of practice C is not as accurate as practice A. This is due to the nonconservation of mass flow rate in practice C. Further, we made calculations for Re = 5,000 with a denser mesh, $25 \times 25$. Figure 5 shows that the performance of practice C is much worse than those of practices A and B, and practice A is better than practice B. This indicates that nonconservation of mass flow rate decreases accuracy greatly. In addition, the nonconservation property may result in unphysical solution. We can assume that the cavity walls are held at a constant temperature $T = 1$ and the dimensionless conductivity is set as $1/\text{Re}$. Then, by solving the energy equation, we should obtain a uniform temperature field $T = 1$. Figure 6 shows the temperature profiles along the horizontal centerline of the square cavity. It is clear that practices A and B reach exact solution $T = 1$, but the solution from practice C is quite unphysical. This is due to the term $A_b$, which can be considered as a false source term due to nonconservation of mass flow rate. From the above test we can draw a conclusion: momentum interpolation is better to use in the three roles of the cell-face velocities to achieve accurate numerical solution. In test 2, practice A is used.

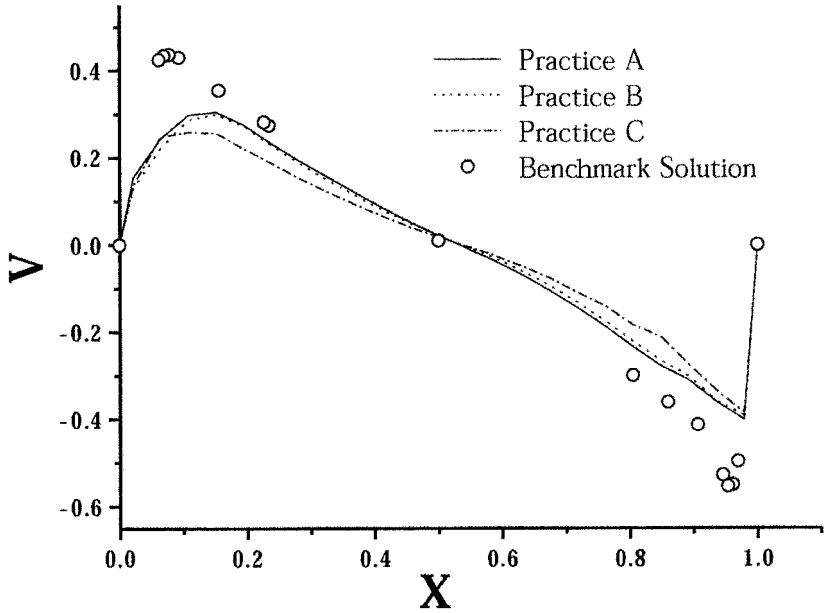


**Figure 5.** Velocity profiles along the horizontal cavity centerline for practices A, B, and C using a $25 \times 25$ uniform mesh for Re = 5,000.

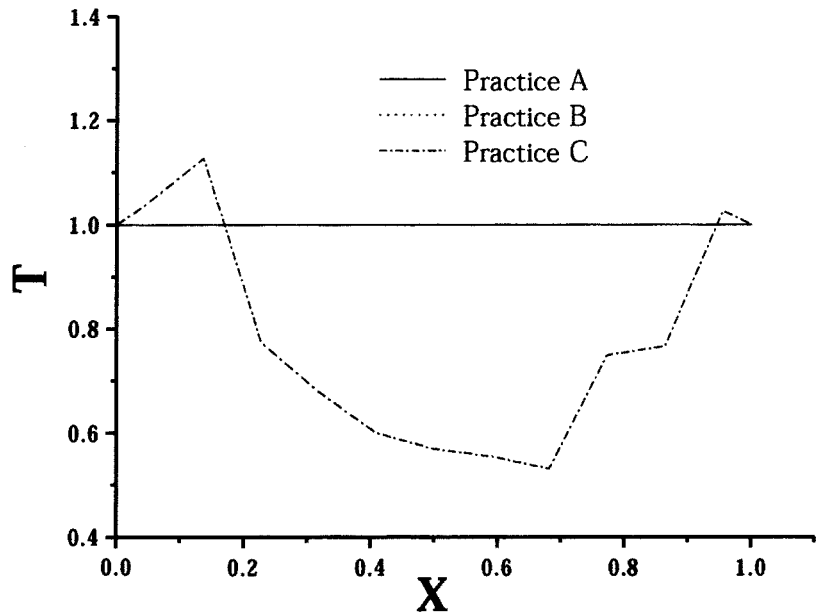


**Figure 6.** Temperature profiles along the horizontal cavity centerline for practices A, B, and C using a $13 \times 13$ uniform mesh for Re = 1,000.

**Table 1.** Effects of underrelaxation factor and time step size on the converged solution using Choi's scheme. Calculations were carried out for a lid-driven cavity problem for Re = 1,000 with $12 \times 12$ mesh. The monitored velocity component $u^*$ is $U(X = 0.65,\ Y = 0.65)$

| $\Delta t$ \ $\alpha_{u,v}$ | 0.1 | 0.5 | 0.7 |
|---|---|---|---|
| 0.1 | 0.0712582 | 0.0712582 | 0.0712582 |
| 1 | 0.0676522 | 0.0676522 | 0.0676522 |
| $10^{30}$ | 0.0641703 | 0.0641703 | 0.0641703 |

**Table 2.** Effects of underrelaxation factor and time step size on the converged solution using the MMIM1 scheme. Calculations were carried out for a lid-driven cavity problem for Re = 1,000 with $12 \times 12$ mesh. The monitored velocity component $u^*$ is $U(X = 0.65,\ Y = 0.65)$

| $\Delta t$ \ $\alpha_{u,v}$ | 0.1 | 0.5 | 0.7 |
|---|---|---|---|
| 0.1 | 0.0721523 | 0.0721523 | 0.0721523 |
| 1 | 0.0721523 | 0.0721523 | 0.0721523 |
| $10^{30}$ | 0.0721523 | 0.0721523 | 0.0721523 |

## Test 2

As indicated above, the present authors reported by a numerical example that solution using Choi's scheme is still time step size-dependent [8]. Here a numerical experiment for Re = 1,000 of the above problem is presented to further demonstrate our analysis. Table 1 shows the numerical results with various time step sizes and velocity underrelaxation factors by using Choi's scheme. From Table 1, we can see that the solutions are independent of velocity underrelaxation factor but dependent on the time step size. The solution difference for various time step sizes cannot be negligible. Our previous report [8] shows that the solution differences of lid-driven cavity flow at various time steps can be negligible for Re = 100 using a

**Table 3.** Effects of underrelaxation factor and time step size on the converged solution using the MMIM2 scheme. Calculations were carried out for a lid-driven cavity problem for Re = 1,000 with $12 \times 12$ mesh. The monitored velocity component $u^*$ is $U(X = 0.65,\ Y = 0.65)$

| $\Delta t$ \ $\alpha_{u,v}$ | 0.1 | 0.5 | 0.7 |
|---|---|---|---|
| 0.1 | 0.0750895 | 0.0750895 | 0.0750895 |
| 1 | 0.0750895 | 0.0750895 | 0.0750895 |
| $10^{30}$ | 0.0750895 | 0.0750895 | 0.0750895 |

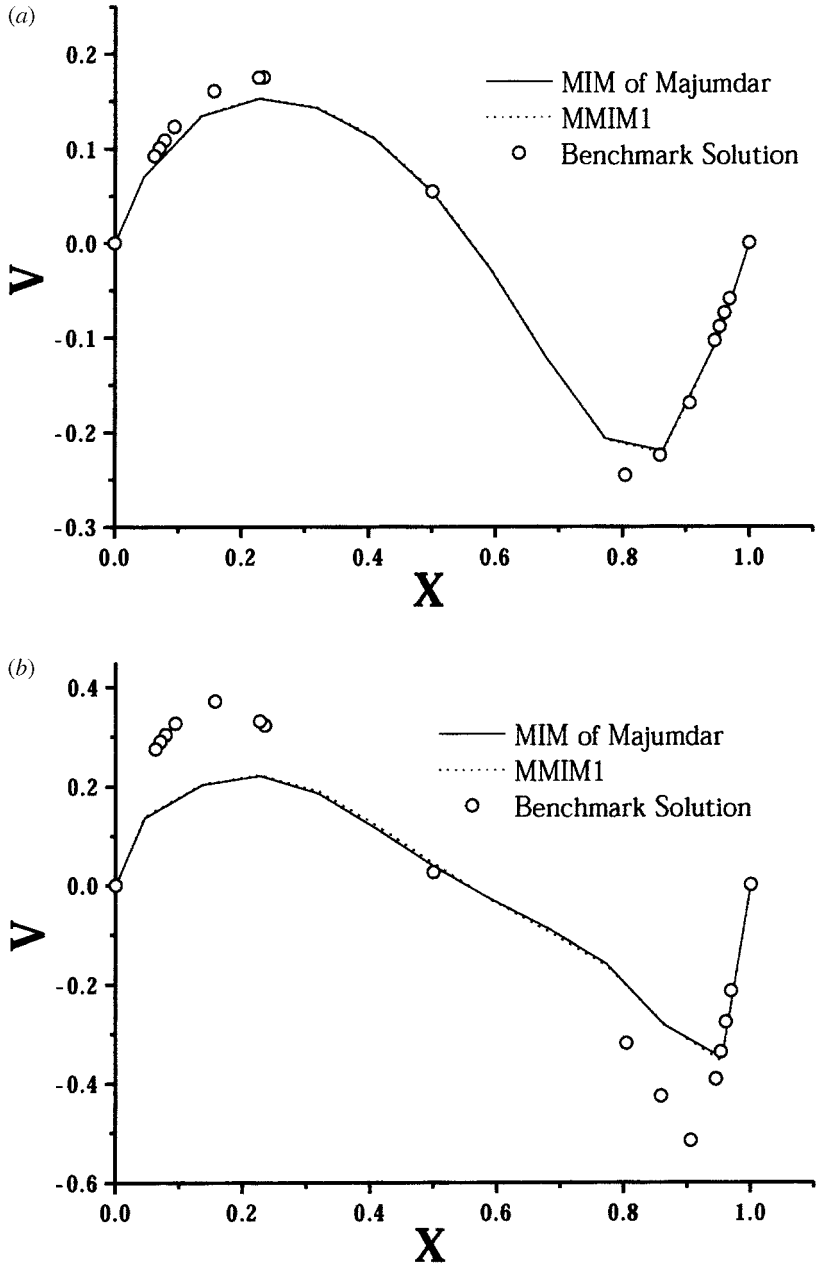


**Figure 7*a–b*.** Velocity profiles along the horizontal cavity centerline for the MIM of Majumdar and MMIM1 using a $13 \times 13$ uniform mesh: (*a*) Re = 100; (*b*) Re = 1,000.

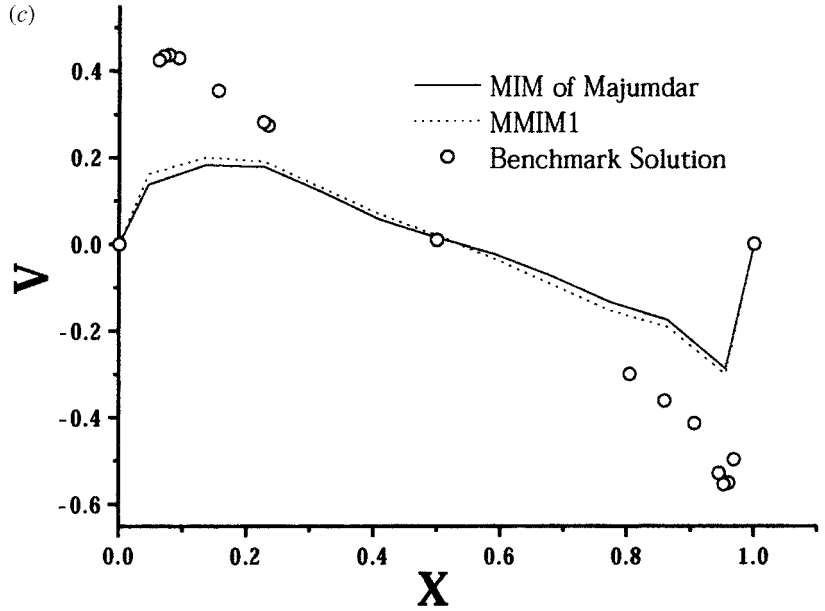


**Figure 7c.** Velocity profiles along the horizontal cavity centerline for the MIM of Majumdar and MMIM1 using a $13 \times 13$ uniform mesh: (*c*) Re = 5,000.

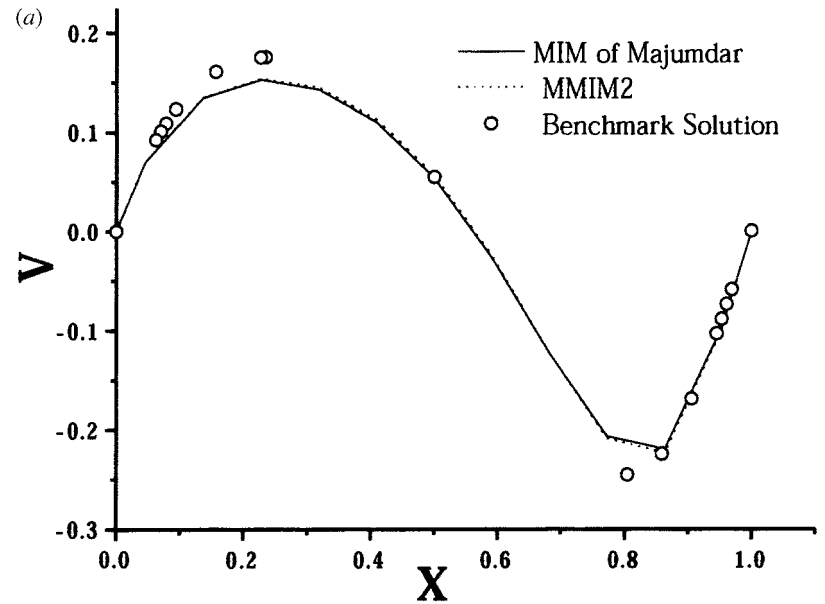


**Figure 8a.** Velocity profiles along the horizontal cavity centerline for the MIM of Majumdar and MMIM2 using a $13 \times 13$ uniform mesh: (*a*) Re = 100.

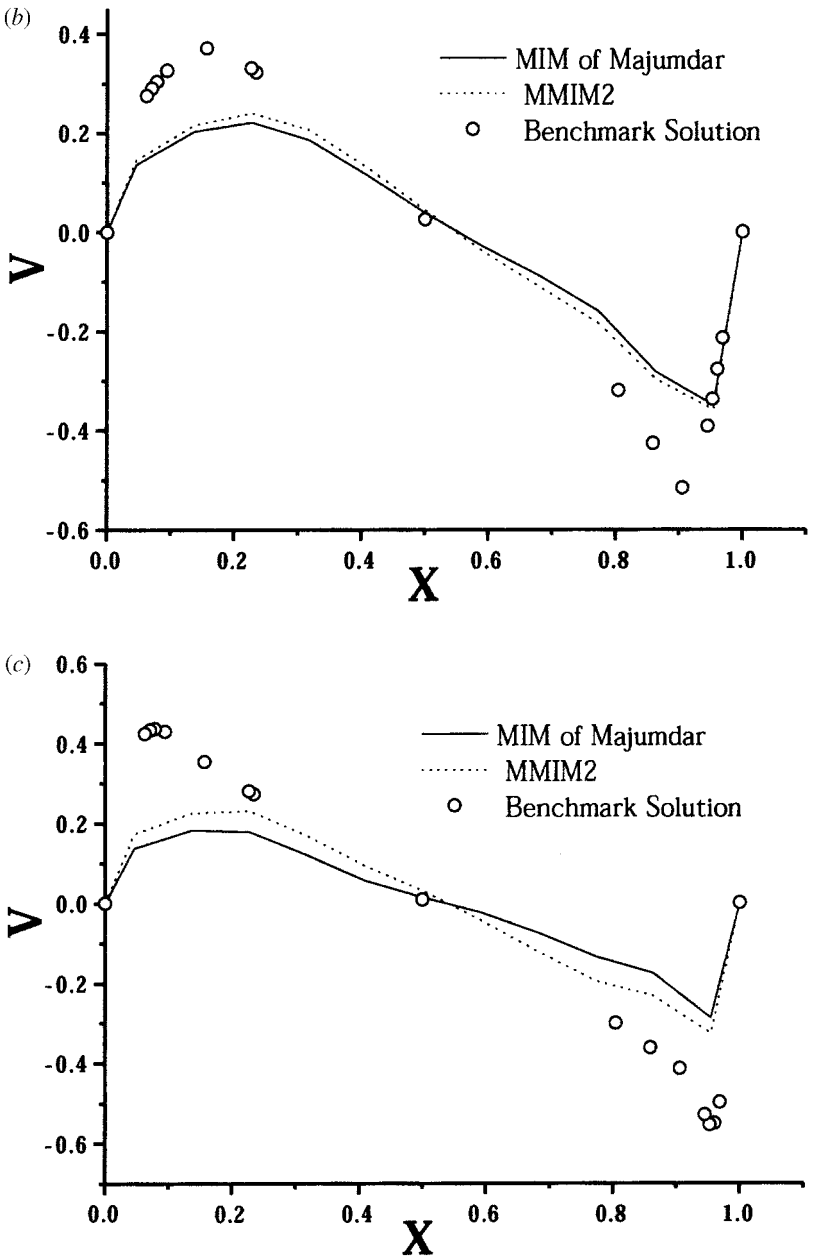


**Figure 8*b*–*c*.** Velocity profiles along the horizontal cavity centerline for the MIM of Majumdar and MMIM2 using a $13 \times 13$ uniform mesh: (*b*) Re = 1,000; (*c*) Re = 5,000.

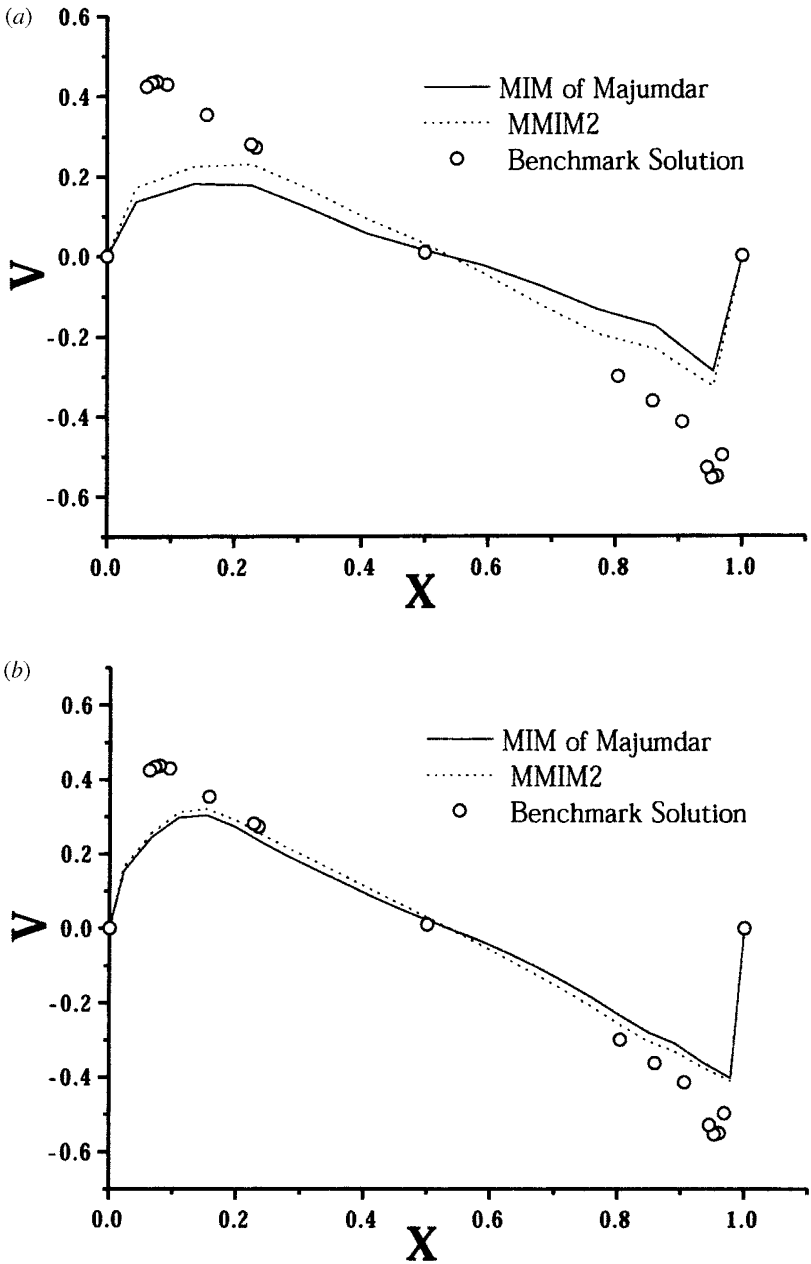


**Figure 9*a–b*.** Velocity profiles along the horizontal cavity centerline for the MIM of Majumdar and MMIM2 for Re = 5,000: (*a*) $13 \times 13$ uniform mesh; (*b*) $25 \times 25$ uniform mesh.

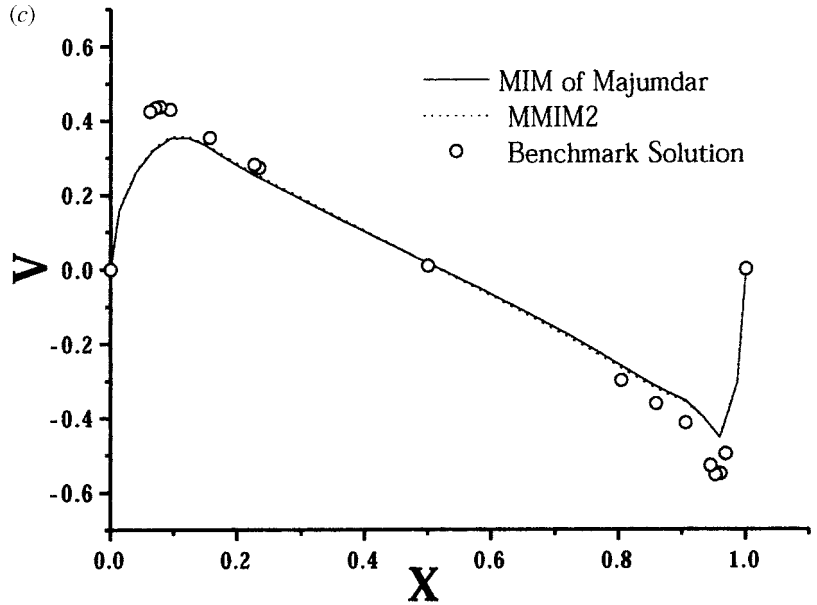


**Figure 9c.** Velocity profiles along the horizontal cavity centerline for the MIM of Majumdar and MMIM2 for Re = 5,000: (*c*) $39 \times 39$ uniform mesh.

power-law scheme and a $22 \times 22$ mesh. The present results shows that when a coarser mesh and the QUICK scheme are employed for a higher Reynolds number, the solution becomes sensitive to the time step size. Thus it is necessary to remove this undesirable feature. Tables 2 and 3 show the numerical results using MMIM1 and MMIM2. It can be seen that the converged solution using these schemes is independent of both relaxation factor and time step size. Figure 7 compares the performance of the MIM of Majumdar [Eq. (25)] and MMIM1 for three Reynolds numbers, Re = 100, 1,000, and 5,000. A uniform grid of $13 \times 13$ mesh is employed. It is clear that for Re = 100 and Re = 1,000, the performance of MMIM1 is slightly more accurate. For Re = 5,000, the advantage of MMIM1 can be observed more clearly.

Figure 8 shows comparisons of the predicted vertical velocity profiles along the horizontal cavity centerline for Reynolds numbers 100, 1,000, and 5,000 by the MIM of Majumdar and MMIM2. A uniform grid of $13 \times 13$ mesh is employed. The comparisons show that more accurate results are predicted by the MMIM2 scheme. The larger the Reynolds number, the larger is the difference between the two schemes. The effect of grid number is studied for Re = 5,000. Three sets of uniform grids ($13 \times 13$, $25 \times 25$, and $39 \times 39$ mesh) are used. The results are shown in Figure 9. It is clear that MMIM2 achieves more accurate results than MIM [Eq. (25)]. With the increase of grid number, the difference between the two schemes becomes smaller. Figure 10 shows the results for Re = 5,000 using a nonuniform $89 \times 89$ mesh with a denser mesh near the walls. It can be seen that the results predicted by the two schemes agree well with the benchmark solution.

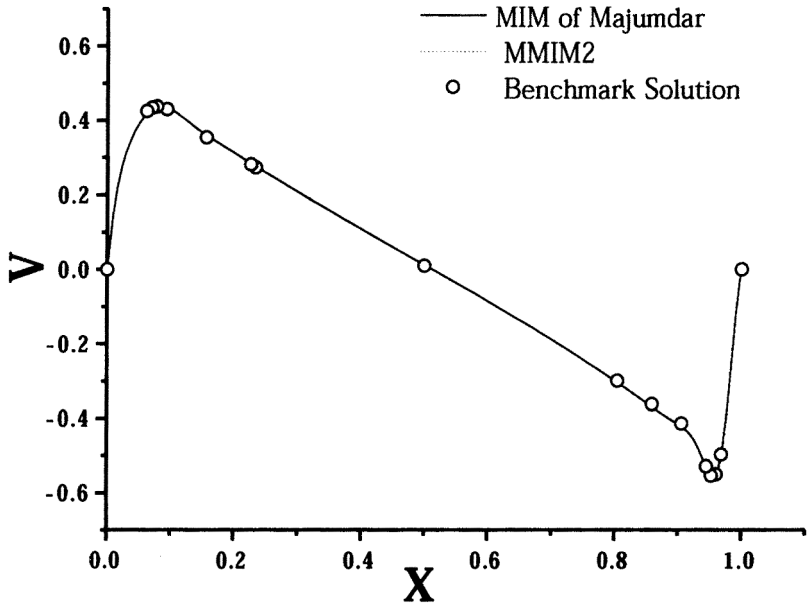


**Figure 10.** Velocity profiles along the horizontal cavity centerline for the MIM of Majumdar and MMIM2 using an $89 \times 89$ nonuniform mesh for Re = 5,000.

## CONCLUSION

Momentum interpolation is better to use to evaluate the cell-face velocities not only in the mass-source evaluation but also in the evaluation of coefficients of the discretization equation. Majumdar's and Choi's momentum interpolation methods are underrelaxation factor-independent but time-step size-dependent. Two new interpolations, MMIM1 and MMIM2, are proposed in this study. Both the mathematical analysis and numerical examples show that the new proposed momentum interpolations are independent of not only underrelaxation factor but also time step size. Numerical simulation for lid-driven cavity flow shows that the accuracy of MMIM1 is similar to that of Majumdar's scheme; and MMIM2 predicts better results than Majumdar's scheme when the grid is not fine as compared to the benchmark solution.

## REFERENCES

1. C. M. Rhie and W. L. Chow, Numerical Study of the Turbulent Flow Past an Airfoil with Trading Edge Separation, *AIAA J.*, vol. 21, no. 11, pp. 1525–1535, 1983.
2. M. Peric, A Finite Volume Method for the Prediction of Three-Dimensional Fluid Flow in Complex Ducts, Ph.D. thesis, University of London, London, UK, 1985.
3. S. Majumdar, Development of a Finite-Volume Procedure for Prediction of Fluid Flow Problems with Complex Irregular Boundaries, Rep. 210/T/29, SFB210, University of Karlsrule, Germany, 1986.
4. S. Majumdar, Role of Underrelaxation in Momentum Interpolation for Calculation of Flow with Nonstaggered Grids, *Numer. Heat Transfer*, vol. 13, pp. 125–132, 1988.

5. T. F. Miller and F. W. Schmidt, Use of a Pressure-Weighted Interpolation Method for the Solution of Incompressible Navier–Stokes Equations on a Non-Staggered Grid System, *Numer. Heat Transfer*, vol. 14, pp. 213–233, 1988.
6. M. H. Kobayashi and J. C. F. Pereira, Numerical Comparison of Momentum Interpolation Methods and Pressure-Velocity Algorithm Using Nonstaggered Grids, *Commun. Appl. Numer. Meth.*, vol. 7, pp. 173–196, 1991.
7. S. K. Choi, Note on the Use of Momentum Interpolation Method for Unsteady Flows, *Numer. Heat Transfer A*, vol. 36, pp. 545–550, 1999.
8. B. Yu, Y. Kawaguchi, W. Q. Tao, and H. Ozoe, Checkerboard Pressure Predictions Due to the Underrelaxation Factor and Time Step Size for a Nonstaggered Grid with Momentum Interpolation Method, *Numer. Heat Transfer B*, vol. 41, no. 1, pp. 85–94, 2002.
9. A. W. Date, Complete Pressure Correction Algorithm for Solution of Incompressible Navier–Stokes Equations on a Nonstaggered Grid, *Numer. Heat Transfer B*, vol. 29, pp. 441–458, 1996.
10. C. Y. Gu, Computation of Flows with Large Body Forces, in C. Taylor, J. H. Chin, and G. M. Homsy (eds.), *Numerical Methods in Laminar and Turbulent Flow*, Pineridge Press, Swansea, UK, 1991.
11. M. M. Rahman, A. Miettinen, and T. Siikonen, Modified Simple Formulation on a Collocated Grid with an Assessment of the Simplified QUICK Scheme, *Numer. Heat Transfer B*, vol. 30, pp. 291–314, 1996.
12. T. Gjesdal and M. E. H. Lossius, Comparison of Pressure Correction Smoothers for Multigrid Solution of Incompressible Flow, *Int. J. Numer. Meth. Fluids*, vol. 25, pp. 393–405, 1997.
13. M. C. Melaaen, Calculation of Fluid Flows with Staggered and Non-Staggered Curvilinear Non-Orthogonal Grids—A Comparison, *Numer. Heat Transfer B*, vol. 21, pp. 21–39, 1992.
14. S. K. Choi, N. H. Yun, and M. Cho, Use of Staggered and Nonstaggered Grid Arrangements for Incompressible Flow Calculations on Nonorthogonal Grids, *Numer. Heat Transfer B*, vol. 25, pp. 193–204, 1994.
15. S. K. Choi, N. H. Yun, and M. Cho, Systematic Comparison of Finite Volume Methods with Staggered and Nonstaggered Grid Arrangements, *Numer. Heat Transfer B*, vol. 25, pp. 205–221, 1994.
16. J. Papageorgakopoulos, G. Arampatzis, D. Assimacopoulos, and N. C. Markatos, Enhancement of the Momentum Interpolation Method on Non-Staggered Grids, *Int. J. Numer. Meth. Fluids*, vol. 33, pp. 1–22, 2000.
17. G. D. Thiart, Improved Finite-Difference Scheme for the Solution of Convection-Diffusion Problems with the SIMPLEN Algorithm, *Numer. Heat Transfer B*, vol. 18, pp. 81–95, 1990.
18. G. D. Thiart, Finite-Difference Scheme for the Numerical Solution of the Fluid-Flow and Heat-Transfer Problems on Nonstaggered Grids, *Numer. Heat Transfer B*, vol. 17, pp. 43–62, 1990.
19. Q. W. Wang, J. G. Wei, and W. Q. Tao, An Improved Numerical Algorithm for Solution of Convective Heat Transfer Problems on Nonstaggered Grid System, *Heat and Mass Transfer*, vol. 33, pp. 273–280, 1998.
20. S. V. Patankar, *Numerical Heat Transfer and Fluid Flow*, Hemisphere, Washington, DC, 1980.
21. B. P. Leonard, A Stable and Accurate Convective Modelling Procedure Based on Quadratic Upstream Interpolation, *Comput. Meth. Appl. Mech. Eng.*, vol. 19, pp. 59–98, 1979.
22. T. Hayase, J. A. C. Humphrey, and R. Grief, A Consistently Formulated QUICK Scheme for Fast and Stable Convergence Using Finite-Volume Iterative Calculation Procedure, *J. Comput. Phys.*, vol. 98, pp. 108–118, 1992.

23. P. K. Khosla and S. G. Rubin, A Diagonally Dominant Second-Order Accurate Implicit Scheme, *Comput. Fluids*, vol. 2, pp. 207–218, 1974.
24. S. K. Choi, H. Y. Nam, and M. Cho, Use of the Momentum Interpolation Method for Numerical Solutions of Incompressible Flows in Complex Geometries: Choosing Cell Face Velocities, *Numer. Heat Transfer A*, vol. 23, pp. 21–41, 1993.
25. R. I. Issa and P. J. Oliveira, Numerical Prediction of Phase-Separation in 2-Phase Flow-Through T-Junctions, *Comput. Fluids*, vol. 23, pp. 347–372, 1994.
26. P. J. Oliveira, F. T. Pinho, and G. A. Pinto, Numerical Simulation of Non-Linear Elastic Flows with a General Collocated Finite-Volume Method, *J. Non-Newtonian Fluid Mech.*, vol. 79, pp. 1–43, 1998.
27. U. Ghia, K. N. Ghia, and C. T. Shin, High-Re Solutions for Incompressible Flow Using the Navier–Stokes Equations and a Multigrid Method, *J. Comput. Phys.*, vol. 48, pp. 387–411, 1982.